



Influence of welding parameters and tool geometry on the morphology and mechanical performance of ABS friction stir spot welds

Yinfei Yan¹ · Yifu Shen¹ · Haobin Lei¹ · Junyi Zhuang¹

Received: 28 September 2018 / Accepted: 7 April 2019 / Published online: 18 April 2019
© Springer-Verlag London Ltd., part of Springer Nature 2019

Abstract

In the present paper, a tool with a flat pin was designed and utilized to friction stir spot weld acrylonitrile butadiene styrene sheets. Influences of welding parameters and pin geometries on joint morphology and mechanical performance were investigated. Results showed that rotational speed during plunging and stirring phase exerted a significant influence on the joint surface appearance and cross-sectional morphology while plunge rate and dwell time showed a slight effect. Secondary extrusion ring, rough weld surface, groove defects, and pores were observed under excessive stirring rotational speed. Spot weld diameter enlarged with the increase of the total tool rotation number in the plunging and stirring phase. Joint lap-shear tensile load varied significantly with the variation of the keyhole orientation. The comparison of the joints produced by different pin geometries showed that flat pin was optimal to fabricate joints with larger bonded region and lap-shear tensile load. With the increase of rotational speed or the decrease of plunge rate, joint shear strength reduced. The proper extension of dwell time under moderate rotational speed exerted a slight influence on the joint shear strength but showed a positive effect on the joint fracture load.

Keywords Friction stir spot welding · Acrylonitrile butadiene styrene · Flat pin · Mechanical performance

1 Introduction

Recently, owing to the increased appeal for environmental protection and energy saving, automotive industry was forced to decrease the vehicle weight to improve fuel economy and reduce the emission of greenhouse gas. Polymeric materials which possess low density and enhanced stress-to-weight ratio have attracted more and more attention and are believed to be substitutes for more metal alloys in the automobile industries in the future [1]. Therefore, spot joining technology which is essential in the assembly of automobiles should be developed to effectively join polymeric components. Friction stir spot welding (FSSW) is one of the friction-based spot joining techniques, which was developed in Mazda Motor Corporation in 1993 for aluminum connection [2]. It possesses many

advantages such as low energy cost, no fume emission, and satisfied joint mechanical performance. In recent years, the investigation of FSSW polymeric materials, such as polypropylene (PP) [3–8], polyethylene (PE) [9–11], polyamide (PA) [12, 13], polycarbonate (PC) [14–18], acrylonitrile butadiene styrene (ABS) [19–21], and polymethyl methacrylate (PMMA) [22], has been conducted by many researchers and great achievements have been made.

Influence of welding parameters, including rotational speed, plunge rate, plunge depth, dwell time, and waiting time has been widely reported in previous researches. Bilici et al. [10] reported that the proper increase of rotational speed, plunge depth, and dwell time led to obvious increase of joint lap-shear tensile force, and plunge rate exerted a slight effect on the joint mechanical property. It was also found that the keyhole was filled by molten HDPE when tool was retracted with no solidification time, which in turn caused severe joint thickness reduction. Yan et al. [12] found that excessive rotational speed, plunge rate, plunge depth, and dwell time commonly caused large material extrusion, which resulted in material loss and poor nugget morphology. A period of waiting time was necessary to avoid nugget material pulling out in the retracting phase. Paoletti et al. [15] declared that increased

✉ Yifu Shen
yfshen_nuaa@hotmail.com

¹ College of Materials Science and Technology, Nanjing University of Aeronautics and Astronautics, 29 Jiangjun Road, Nanjing 210016, People's Republic of China

plunge rate led to decreased process temperature and enlarged welding force and torque. Proper increase of rotational speed brought about more frictional heat and promoted material flow, thus leading to enlarged weld area. Increasing dwell time led to higher maximum temperature and larger weld area without significantly influencing the welding force. Lambiase et al. [16] pointed out that increased plunge depth led to the enlargement of bonded region due to larger frictional heat generation. But excessive plunge depth resulted in severe joint thickness reduction, which caused the decrease of joint fracture load. In order to remove thickness reduction, Yan et al. [20] proposed a method of adding polymer gaskets to the weld region before welding operation. It was found that joints without thickness variation showed higher fracture load than that with thickness reduction.

Pin geometry and dimension, shoulder profile and diameter, tool configuration, and so on have been demonstrated to be important to joint formation and mechanical performance. Bilici et al. [6] stated that tapered cylindrical pin was better to produce spot welds with large nugget thickness and high quality compared with other pin geometries. Furthermore, the investigation of tapered pin tool dimension suggested that the proper increase of shoulder diameter, shoulder cavity angle, and pin angle was beneficial to obtain high-strength joints. In another paper [9], the influence of pitch length of threaded pin on PP joint quality was investigated, and it was found that increasing pitch length resulted in decreased joint fracture load. Lambiase et al. [16] reported that increasing shoulder diameter or decreasing pin diameter within a proper range led to larger joint fracture load, but joint shear strength decreased with shoulder diameter. Axial load and torque were negligibly influenced by the taper angle of the pin but obviously increased with the pin and shoulder diameter [17]. Dashatan et al. [19] pointed out that conventional tool and FSSW process always resulted in molten nugget material extrusion and insufficient forge pressure. Therefore, a tool with stationary plate was designed and satisfied spot welds were produced between PMMA and ABS. Large keyhole left by FSSW was a restriction to the promotion of joint strength. In order to reduce the keyhole size, a FSSW tool with triflute pin was designed by Yan et al. [20]. With the assistance of a properly designed clamping plate, ABS joints with keyhole smaller than that produced by conventional cylindrical pin were produced. Friction spot welding (FSpW) was another effective joining method, which was able to remove keyholes. Oliveira et al. [22] employed FSpW technology to join PMMA, through the accurate control of the independent pin and sleeve; joints without keyhole were successfully produced. Gonçalves et al. [13] demonstrated the feasibility of FSpW carbon fiber-reinforced polyamide 66, and joints with strength comparable to that fabricated by ultrasonic welding were obtained. However, the motion of the sleeve and the pin during the FSpW process

should be accurately controlled by extra devices, which undoubtedly increased the cost.

In the present investigation, a tool with a flat pin was fabricated and employed to friction stir spot weld ABS sheets, which aimed at decreasing the keyhole volume. The feasibility of FSSW ABS by flat pin tool was demonstrated first and then the influence of welding parameters on joint morphology and mechanical property was analyzed. What's more, the effect of pin geometries on joint dimension and mechanical performance was determined.

2 Material and methods

ABS plates with the thickness of 6 mm were cut into the length of 150 mm and the width of 60 mm and were fixed on the workbench of a modified milling machine with the overlapped area of $60 \times 60 \text{ mm}^2$. The physical and mechanical properties of ABS sheets were listed in Table 1. Figure 1 a shows the schematic diagram of the FSSW apparatus. A tool with a shoulder and a flat pin was designed and utilized to spot weld ABS sheets. The tool was made of a 1045 steel and the specific dimensions were illustrated in Fig. 1 b and c. An aluminum clamping plate which was characterized with a central through-hole was employed and fixed on the surface of lapped ABS sheets, as shown in Fig. 1 a. The length, width, and thickness of the clamping plate were 240 mm, 60 mm, and 12 mm, respectively. The diameter of the through-hole was determined to be 0.6 mm larger than the shoulder, which aimed at restricting the material extrusion during the welding process.

The steps of FSSW ABS by flat pin tool were illustrated in Fig. 2, including plunging, stirring, solidifying, and retracting. In the beginning, the flat pin tool rotated with prescribed rotational speed (N_p) and plunged into the weld region passing through the through-hole with a predetermined plunge rate (R_p). ABS material was heated and partially substituted by the rotating flat pin during the plunging phase. When shoulder bottom moved near the top surface of the upper sheet, the substituted ABS material was squeezed. Partial material was forced to backfill the nugget zone and another part of material filled the gap between the shoulder and the through-hole. Through the heat conduction to the clamping plate, material inside the gap solidified quickly and then prevented further nugget material extrusion in the stirring phase. Upon the shoulder bottom touching the upper sheet surface, tool vertical

Table 1 The physical and mechanical properties of ABS sheet

Properties	Density (g/cm^3)	Melting point ($^{\circ}\text{C}$)	Tensile strength (MPa)	Elongation (%)
ABS	1.05	217–237	40.8	21

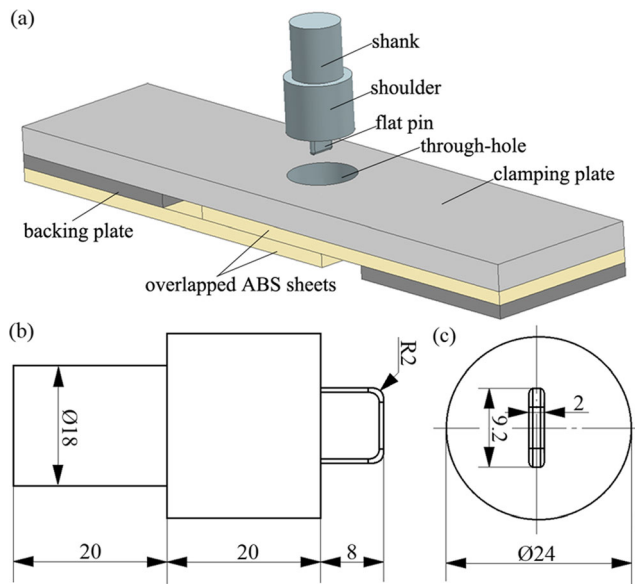


Fig. 1 a The schematic of FSSW ABS sheets by flat pin tool; b, c the specific dimension of the tool (in mm)

plunging was stopped. Different from the researches reported previously [3–10], the tool rotational speed in the stirring phase (N_S) changed, and the duration of the tool stirring was called dwell time (T_D). Tool stopped rotating after the stirring phase and then weld material solidified under the shoulder pressure for a period of time (solidification time, T_S). Finally, the flat pin tool was retracted from the weld region and a spot weld was produced. Figure 2 (A-A) shows the schematic diagram of the weld horizontal section, where D_B is the diameter of the bonded region. T_S was determined to be 25 s after a number of trials in order to avoid the phenomenon of nugget material pulling out in the retracting phase [12].

In the present paper, the influence of N_B , R_B , N_S , and T_D on the joint morphology, dimension, and mechanical property

was investigated. After a number of experimental trials, the experiment was properly arranged, as listed in Table 2. Different from the spot welds reported in previous researches, the keyhole left by the flat pin showed different lengthwise orientations after FSSW. The influence of the angle between keyhole lengthwise orientation and tensile direction (marked by α in Fig. 3) on joint mechanical property should be determined. Therefore, three different keyhole orientations, including $\alpha = 0^\circ$, $\alpha = 45^\circ$, and $\alpha = 90^\circ$ were adopted. It was reported that pin geometry exerted significant influence on the frictional heat generation and material flow, which in turn affected the joint morphology, dimension, and strength [9]. Accordingly, another three tools with cylindrical pin, triangular pin, and triflute pin were adopted to spot weld ABS and a comparison between joints made by various tools was conducted. The tool graphs and the dimensions of three pins were illustrated in Fig. 4. The diameter and length of the shoulders and the length of the pins were the same as the flat pin tool. According to Figs. 1 and 4, the area of the keyholes (A_K) on the bonded region can be calculated, that is 17.54 mm² for flat pin, 66.48 mm² for cylindrical pin, 33.27 mm² for triangular pin, and 20.67 mm² for triflute pin. Therefore, the area of the bonded region (A_B) can be calculated according to Eq. (1):

$$A_B = \frac{\pi \times D_B^2}{4} - A_K \tag{1}$$

where D_B was the diameter of the bonded region and A_K was the area occupied by the keyhole.

Optical microscope was used to observe the joint morphology, and SANS CMT 5105 microcomputer control electronic universal tensile testing machine was adopted to test the lap-shear tensile load (L_T) of the joints made under different welding conditions. The dimension of the lap-shear tensile

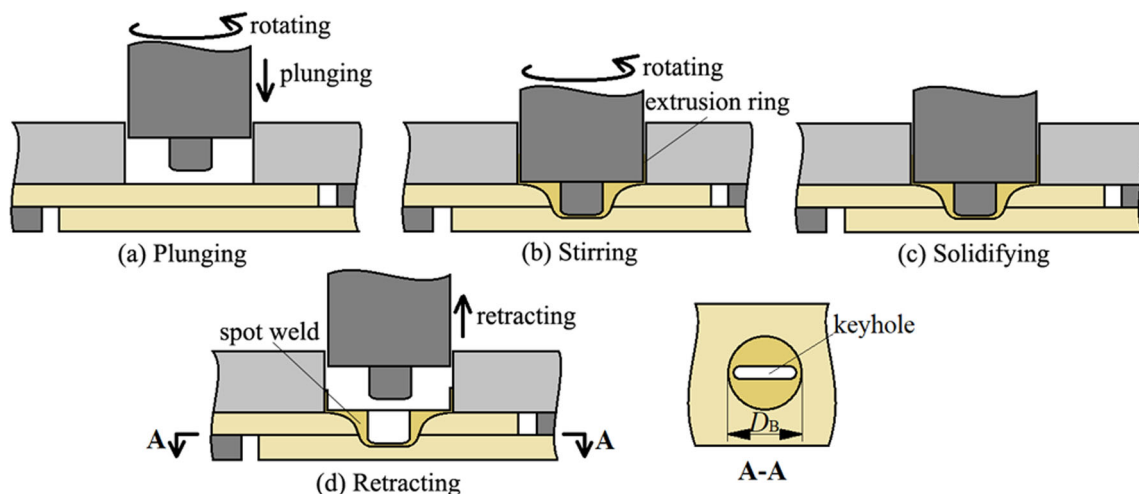


Fig. 2 The process of FSSW ABS sheets: a plunging, b stirring, c solidifying, d retracting; (A-A) the bonded region; D_B the diameter of the bonded region

Table 2 The specific experimental arrangement

Experiment number	Welding parameters			
	N_P (rpm)	R_P (mm/min)	N_S (rpm)	T_D (s)
1	500	10	400	12
2	875	10	400	12
3	1250	10	400	12
4	500	5.71	400	12
5	500	4	400	12
6	500	10	800	6
7	500	10	1200	6
8	500	10	400	6
9	500	10	400	18

specimen was schematized in Fig. 3. Joint shear strength (S_S) was calculated according to the Eq. (2):

$$S_S = \frac{4L_T}{\pi \times D_B^2} \quad (2)$$

Five replicates performed under the same welding condition were fabricated and the average lap-shear tensile load and shear strength were used to assess the joint quality.

3 Results and discussion

3.1 The typical morphology of the spot weld

To reveal the geometry of the spot weld, a cylindrical hole with a diameter and a depth of both 2 mm was drilled at the center of the weld region and graphite powder with the particle size of about 30 μm was added into the hole before welding operation, as in the schematic revealed in Fig. 5 a. Figure 5 b is the cross-section of the joint produced with graphite powder addition. It can be seen that the stir zone (SZ) showed bowl-shaped geometry, which can be explained as follows. Due to the extra frictional heat the shoulder provided, more material in the upper portion of the SZ was softened, which in turn led

to bowl-shaped nugget zone. Furthermore, it was observed that the graphite powder distributed in the most region of SZ, which meant that apparent horizontal and vertical material flow and mixture occurred inside the nugget during the welding process. However, two regions which were different in color from the surrounded nugget material were found at the nugget bottom, as marked in Fig. 5 b. It was possible that softened beige ABS material underneath the bottom of the pin was extruded to flow upwards due to the pin rotating, which led to the formation of embedded morphology at the nugget bottom. Figure 5 c shows an enlarged view of the region marked in Fig. 5 b, where an extra bonded region was observed between the black stir zone and the lapped interface. Such region was generated due to local plastic deformation resulted from conducted heat and extrusion force, which was called thermal-mechanically affected zone (TMAZ).

3.2 The analysis of typical joint crown appearance

Among the spot welds produced according to Table 2, two joint crown appearances were observed, as shown in Fig. 6. Joints fabricated under moderate N_P and N_S possessed regular initial ring and flat surface, as shown in Fig. 6 a. However, the initial ring detached from the weld surface during the welding process when N_P increased to 1250 rpm or N_S was larger than 800 rpm (see Fig. 6 b), where the initial ring encased the shoulder. Simultaneously, secondary extrusion ring was generated in the vicinity of the spot weld and the joint surface became rough, as can be seen in Fig. 6 c. The formation process of the secondary extrusion ring was described in Fig. 7. It was likely that the clamping plate increased the material cooling rate, which kept the thin extrusion ring in solid state even under high rotational speed, as shown in Fig. 7 a. However, high rotational speed meant larger frictional heat input and increased shear effect, which resulted in the more softened ring root and the decreased nugget material viscosity. Furthermore, excessive rotational speed led to larger centrifugal force and extrusion force. In this case, the initial ring was easy to separate from its softened root and was forced to move upwards by the squeezed low-viscosity nugget material, as displayed in Fig. 7 b. The extruded nugget material

Fig. 3 The dimension (in mm) and the keyhole orientation angle (in $^\circ$) of the lap-shear tensile specimen

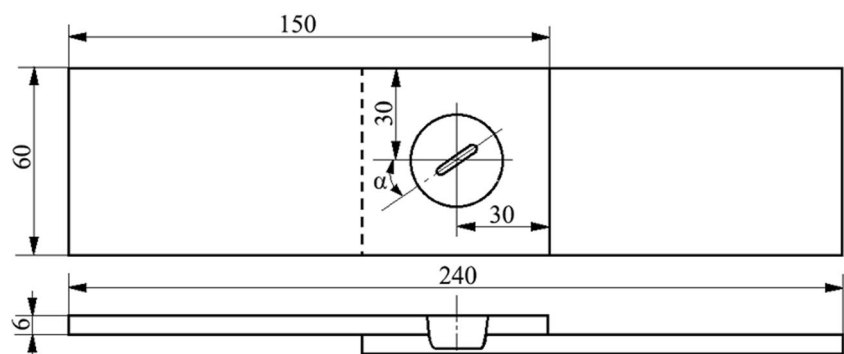
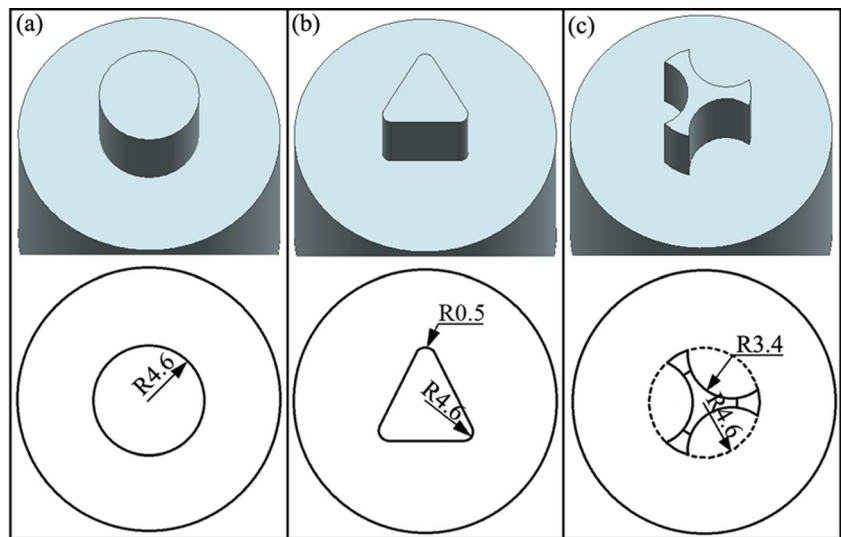


Fig. 4 The geometry and the dimension of tools with **a** cylindrical pin, **b** triangular pin, and **c** triflute pin



solidified rapidly due to the cooling effect of the clamping plate, generating the secondary extrusion ring in the vicinity of the spot weld, as illustrated in Fig. 7 c. In the retracting phase, the initial ring which was detached from the weld surface was taken away from the weld zone, forming the phenomenon displayed in Fig. 6 b. The shoulder pressure decrease resulted from the secondary material extrusion and the possible turbulent material flow caused by the excessive tool stirring were responsible for the rough weld surface shown in Fig. 6 c.

3.3 Influence of welding parameters on the joint morphology and dimension

The cross-sections of the joints produced with various N_p and R_p were displayed in Fig. 8. It was found that defect-free joints were obtained at moderate N_p while groove defects were observed at the bottom corner of the keyhole when N_p increased to 1250 rpm. Also, the groove defects were almost rotationally symmetric, as the right and the left cross-sections of joint 1250/10 illustrated in Fig. 8. Moderate N_p meant proper frictional heat input and extrusion force, so nugget material

squeezing was negligible during the stirring phase and sound joints were fabricated. However, as explained above, high N_p resulted in the secondary extrusion of the nugget material. Therefore, nugget material became insufficient and grooves were generated subsequently. It was worth noting that grooves distributed at the bottom corner of the keyhole. Such phenomenon was closely related to the material flow during and after the stirring phase. Figure 9 a is the schematic diagram of horizontal material flow, showing that cavities were generated at the backside of the rotational flat pin and the cavity size increased along the radius direction because of the radially increased linear velocity of the rotating pin. Simultaneously, it was possible that cavity size increased along the weld depth, as in the schematic displayed in Fig. 9 a (A-A). This was because the circumferential material flow at lower portion of the nugget was mainly dragged by the flat pin while nugget material underneath the shoulder bottom was dragged by both the rotating shoulder and the pin. Therefore, the cavity at the lower portion of the nugget was larger than that at the upper portion. In this case, cavities tended to be gradually filled from inner to outer along the radial direction and from top to bottom along the weld depth, which then resulted in the groove

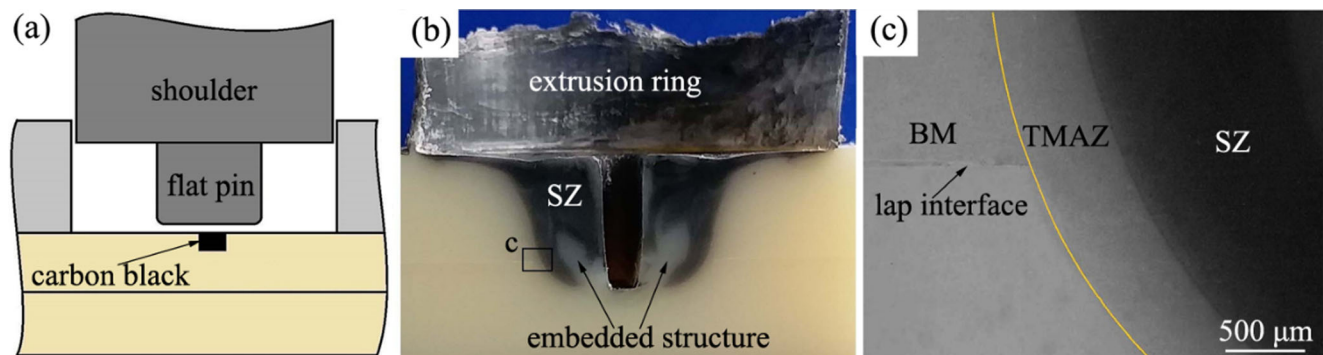
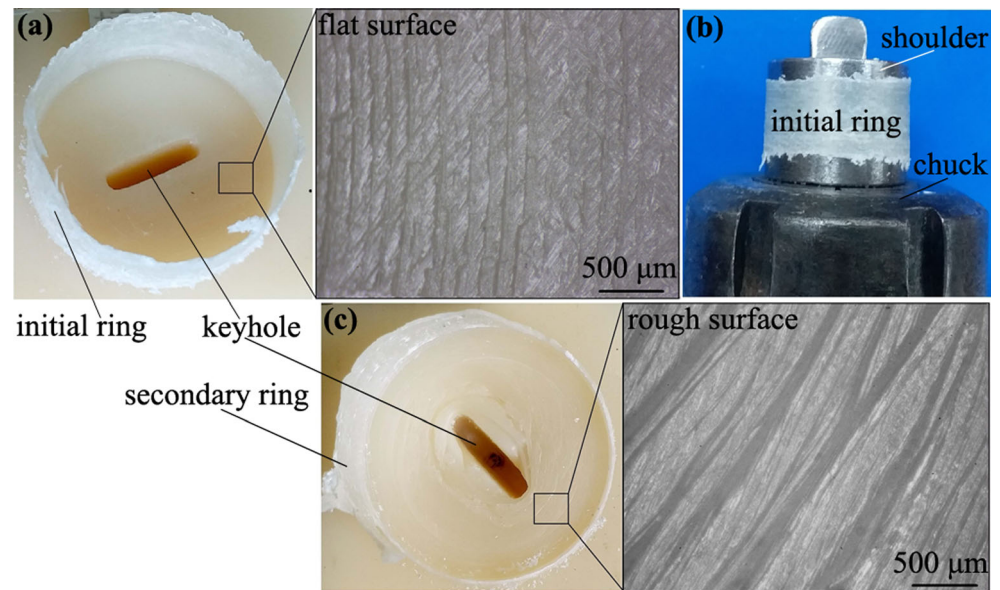


Fig. 5 **a** The schematic of graphite powder addition, **b** the joint cross-sectional geometry, and **c** the division of the spot weld

Fig. 6 **a** Spot welds with initial ring and flat surface, **b** the separated initial ring, and **c** spot welds with secondary ring and rough surface



generation at the bottom corner of the keyhole. What's more, it was considered that cavity filling after the stirring phase significantly affected the groove geometry. Figure 9 b is the schematic diagram of material filling the moment after stirring phase. Backflow filling from two ends of the flat pin and extrusion filling from the near side of the flat pin happened simultaneously. According to bowl-shaped joint cross-section shown in Fig. 5 b, it was suggested that backing flow filling at the upper portion of the nugget was larger than that occurred at the lower portion. In this case, cavity at the upper region of the weld was easier to be fully filled than that at the lower region.

The influence of N_S and T_D on joint cross-sectional morphology was clearly revealed in Fig. 10. It was found that N_S exerted a significant influence on the joint formation while T_D showed slight effect on the weld morphology. Small N_S was beneficial to the production of spot welds with no visible defects and enlarged N_S resulted in the emergence and the increase of groove defects. Obviously, the frictional heat generation was moderate at N_S of 400 rpm and the initial extrusion ring was stable, which effectively restricted the material loss during the stirring phase. However, a larger N_S led to severer material viscosity decrease and increased extrusion

force and centrifugal force. Initial ring was forced to detach from the weld surface and secondary ring was generated, which resulted in more material squeezing and enlarged groove defect. In addition to the increased groove defect at N_S of 1200 rpm, many pores with various sizes were generated and distributed along the boundary of the nugget, as in the magnification shown in Fig. 10 (I). On the one hand, excessive material loss at the extreme N_S caused the forge pressure decrease, thus leading to the decrease of weld compactness. On the other hand, severe shear effect and excessive friction heat input under large N_S may cause material degradation, which in turn resulted in the formation of pores. Sound joints were fabricated under various dwell times, as demonstrated in Fig. 10. Owing to the low N_S of 400 rpm, proper increase of T_D did not cause heavy material viscosity decrease nor initial extrusion ring detaching, so material loss did not increase with the extension of dwell time and no visible defects were generated.

Figure 11 shows that the diameter of the bonded region consisted of three parts, including left width, middle width, and right width. The middle width was 9.2 mm and the left and right width can be obtained through the corresponding

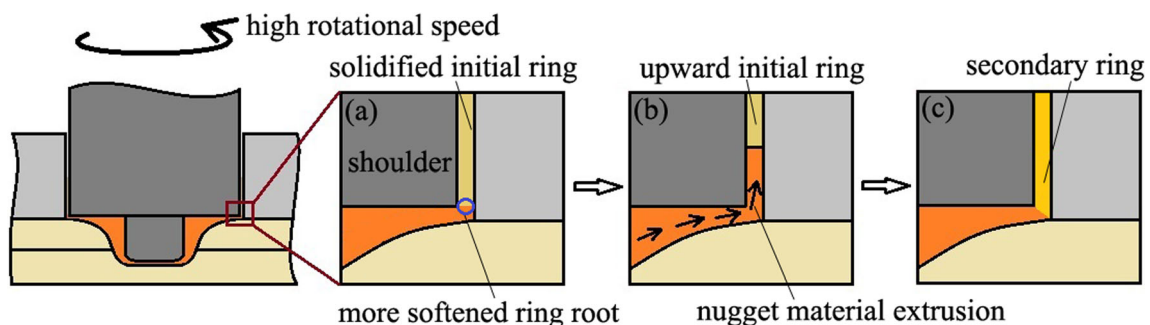


Fig. 7 The schematic of secondary ring formation process under high rotational speeds

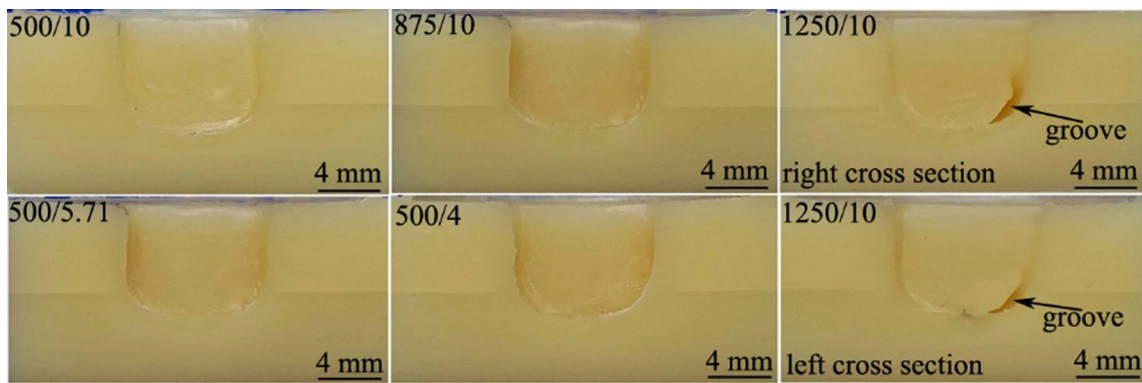


Fig. 8 The variation of joint cross-sectional morphology with N_p/R_p

optical graphs. The influence of welding parameters on the diameter of the bonded region was investigated. Figure 12 a and b present the line charts concerning the variation of bonded region diameter towards N_p , R_p , N_s , and T_D . It was found that N_p and R_p exerted different influences on the bonded region dimension although the total rotation number enlargement was the same. The increase of D_B from N_p500 to N_p875 was larger than that from N_p875 to N_p1250 . It was the reason that excessive N_p may cause severe material extrusion through the shoulder bottom during the tool plunging, which in turn reduced the frictional heat generation and then caused the decreased enlargement of D_B from N_p875 to N_p1250 . Increasing the tool rotation number through decreasing R_p led to more frictional heat generation without causing excessive material extrusion, as confirmed by the cross-sectional morphology shown in Fig. 8, where no groove defect was generated under different R_p values. So spot weld diameter enlarged linearly with the decrease of plunge rate. It was observed from Fig. 12 b that the increase of tool rotation number through increasing the rotational speed or propagating the dwell time led to the enlargement of the joint size. Similarly, increased heat input and material stirring resulted from more tool rotation was responsible for the enlargement of the spot

weld diameter. However, it was noted that the increment of D_B from N_s800 to N_s1200 became small compared with that from N_s400 to N_s800 , which was similar to the phenomenon occurred to N_p . On the one hand, the viscosity of the nugget material was further decreased under excessive N_s due to larger heat input and stronger shear effect, which caused the reduction of frictional heat generation efficiency [23]. Furthermore, shoulder pressure may decrease due to more nugget material extrusion under excessive N_s . In this case, the friction heat generation did not increase obviously although N_s increased from 800 to 1200 rpm, which caused the slowing down of the D_B increment.

3.4 Influence of keyhole orientation on joint lap-shear tensile load

Different from the spot welds produced by tools with cylindrical pin or tapered pin under conventional FSSW process [3–11], the joint produced by flat pin showed different keyhole orientations. In order to determine the influence of keyhole orientation on joint mechanical performance, three kinds of joints with $\alpha 0^\circ$, $\alpha 45^\circ$, $\alpha 90^\circ$ were fabricated and the corresponding lap-shear tensile loads were tested. Figure 13

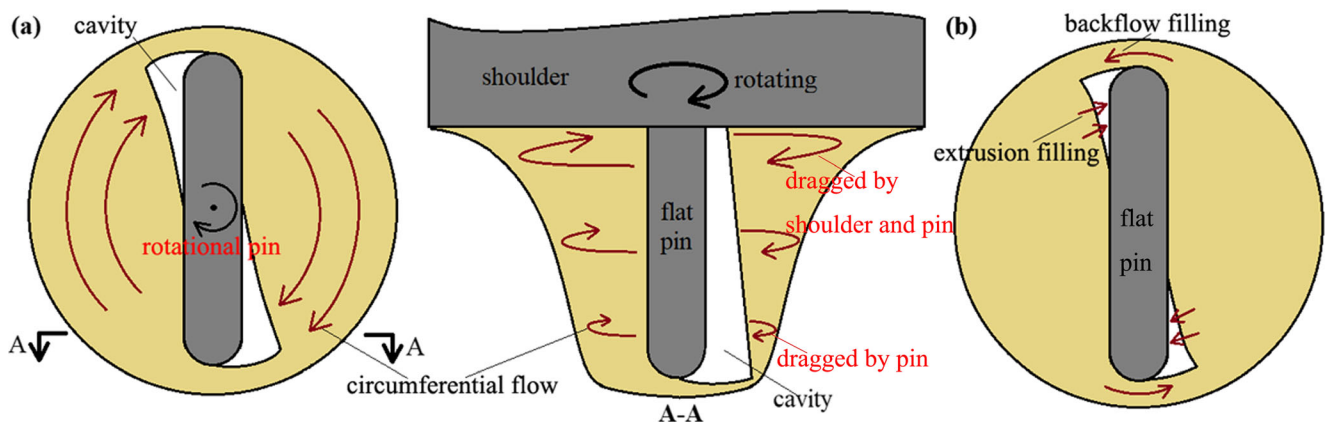


Fig. 9 The schematics of the horizontal (a) and vertical cross-sections (A-A) of the nugget zone during stirring phase; b material filling the moment after stirring phase

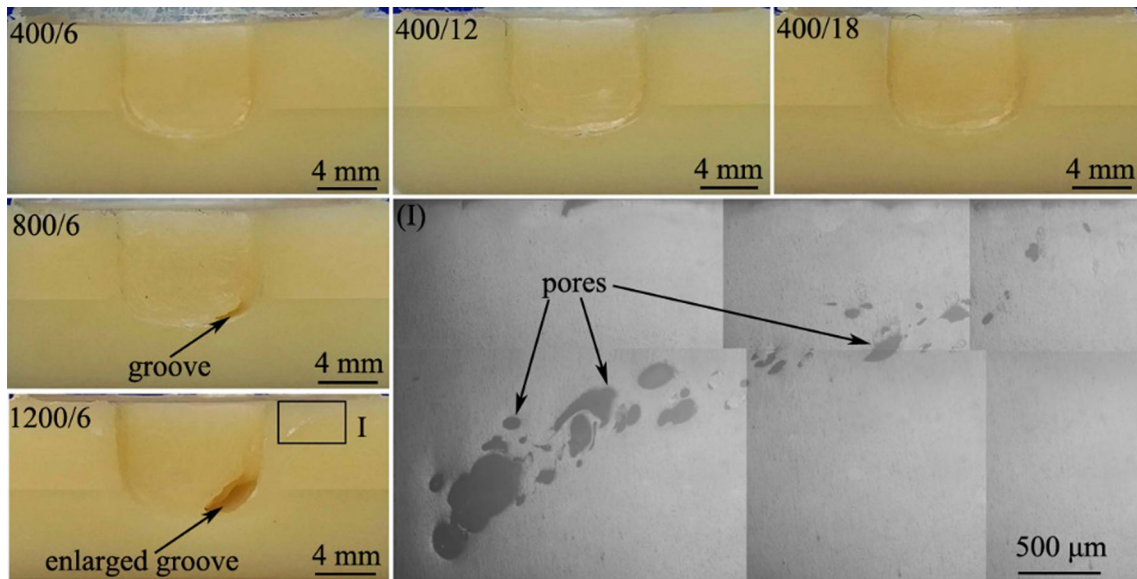


Fig. 10 The cross-sectional morphology variation towards N_s/T_D ; (I) the optical micrograph of the marked region I

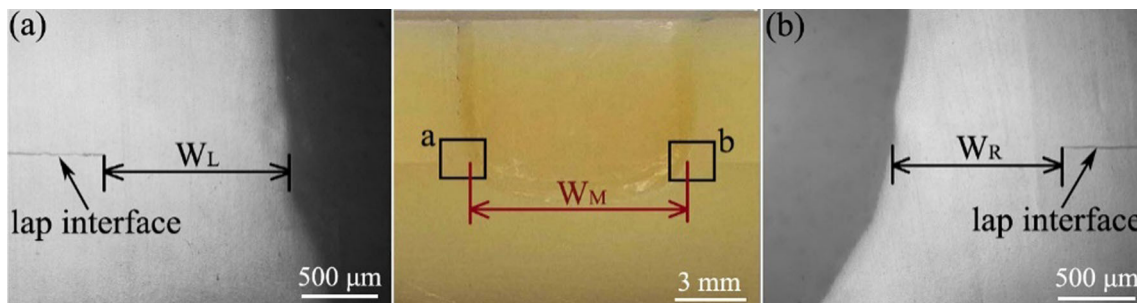


Fig. 11 a Left width, b middle width, and c right width of the joint bonded region

a reveals that joint lap-shear tensile load reduced with the increase of α . Generally, the tensile force (F) can be divided into F_V (vertical to keyhole orientation) and F_P (parallel to keyhole orientation) during the tensile test, as illustrated in Fig. 13 b (I). The width of the bonded region at two ends of the keyhole was small. Therefore, cracks initiated at the tip of

the lap interface due to stress concentration propagated quickly under F_V and eventually caused the local separation in advance, as in the schematic illustrated in Fig. 13 b (II). Increased α meant enlarged F_V under the same tensile load, which increased the crack propagation inside the bonded region at keyhole ends. Therefore, larger α caused local

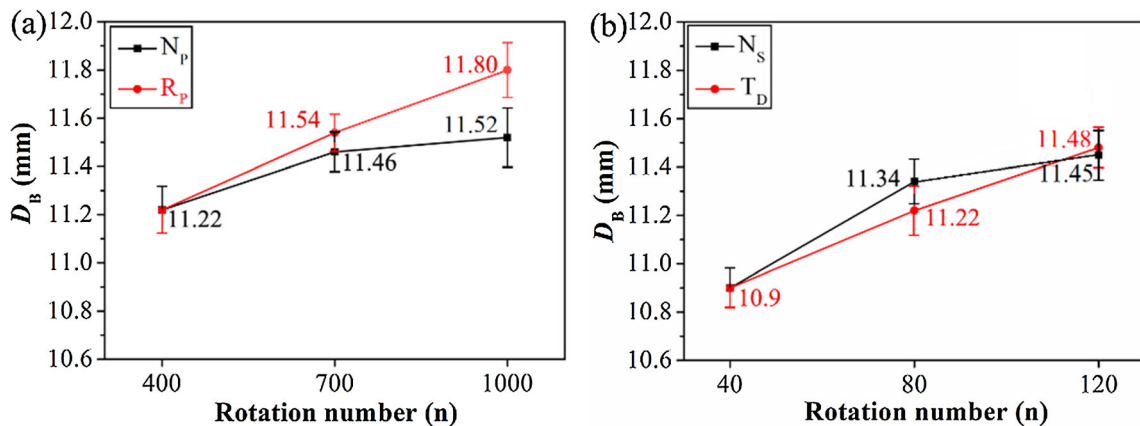


Fig. 12 Influence of a N_p and R_p and b N_s and T_D on bonded region diameter

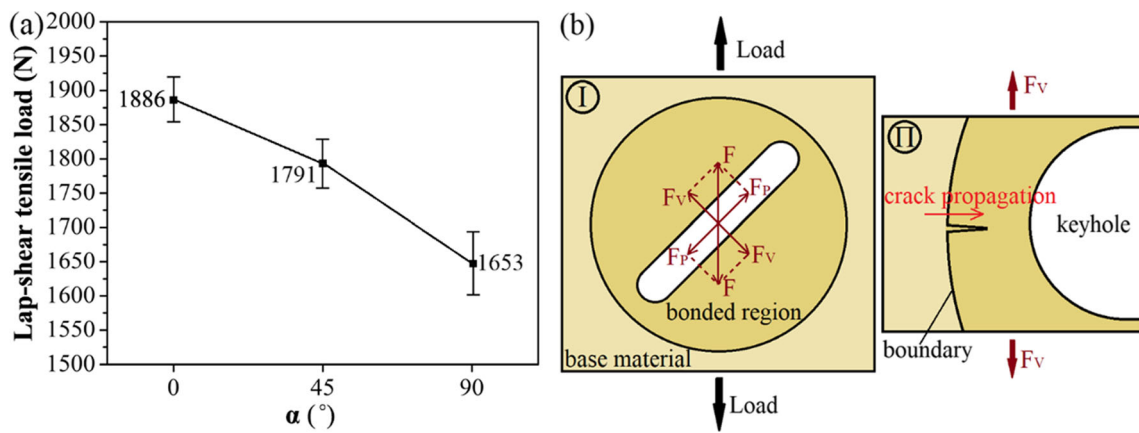


Fig. 13 a The variation of joint lap-shear tensile load towards α and b the force analysis of the bonded region in the tensile tests

separation at two ends of the keyhole ahead of time, which in turn accelerated the failure of the joints and resulted in the decrease of joint fracture load.

3.5 Influence of pin profiles on joint formation and mechanical property

The surface appearances and the cross-sections of the spot welds produced by tools with cylindrical pin, triangular pin, triflute pin, and flat pin under the same N_P of 500 rpm, R_P of 10 mm/min, N_S of 400 rpm, and T_D of 12 s were displayed in Fig. 14 a. It was observed that all spot welds showed smooth surface appearance and defect-free cross-sectional morphology. The profiles of the pins were accurately transferred onto the joints, forming keyholes with different geometries and

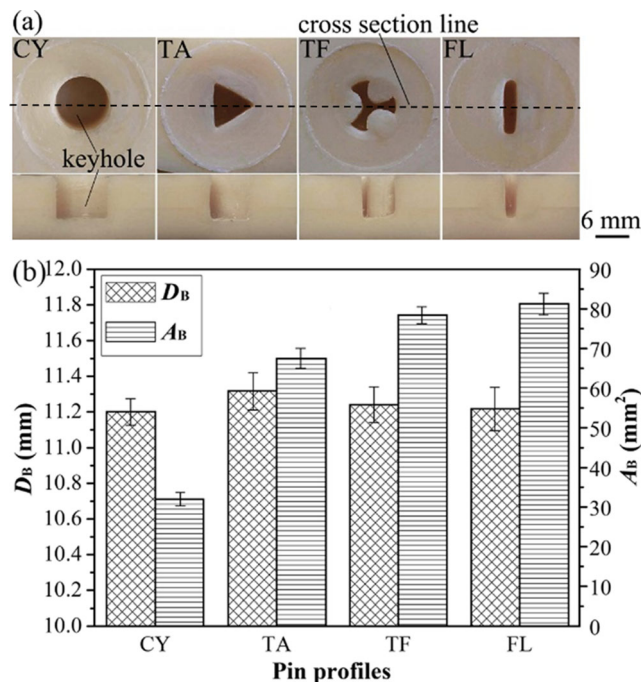


Fig. 14 a The surface appearances and cross-sections and b the D_B and A_B of four joints fabricated by different pins

dimensions. The larger the pin, the bigger the keyhole. Figure 14 b shows the diameter and the area of the bonded regions produced by four pins. It was found that D_B of the joints fabricated by triangular pin was 11.32 mm, which was larger than that produced by other tools. On the one hand, it was reported that the axial pressure increased with the pin bottom dimension [17]. On the other hand, the material has been substituted by a triangular pin was larger than triflute pin and flat pin, which caused more material extrusion and led to an increased shoulder pressure. Therefore, more frictional heat was generated with the triangular pin, thus leading to more material softening and larger D_B . Although the pin bottom area and the material been substituted by cylindrical pin were both the largest, the corresponding D_B was similar to that obtained by triflute pin and flat pin. Such phenomenon may attribute to the fact that cylindrical pin was weak to drag material to flow during the welding process. According to Eq. (1), A_B of joints produced by four tools were calculated, as shown in Fig. 14 b. It was found that cylindrical pin tool produced joints with the smallest bonded region due to the largest keyhole, and joints fabricated by flat pin tool whose pin size was the smallest showed the largest A_B . The fracture surface morphology of four joints was presented in Fig. 15 a, suggesting that all joints failed with shear fracture mode. Figure 15 b is the load verse displacement curves of four typical joints. It was suggested that joints fabricated by flat pin tool showed the maximum fracture load and displacement while cylindrical pin tool produced joints with poor mechanical property. Combined with Fig. 14 b, it was found that the joint lap-shear tensile load enlarged with the increased A_B , which meant that optimizing the pin geometry to increase the A_B was an effective way to promote the joint performance.

3.6 Effect of welding parameters on joint L_T and S_S

Lap-shear tensile tests were carried out to assess the mechanical performance of the joints produced under various welding parameters. It was found that all joints failed with shear

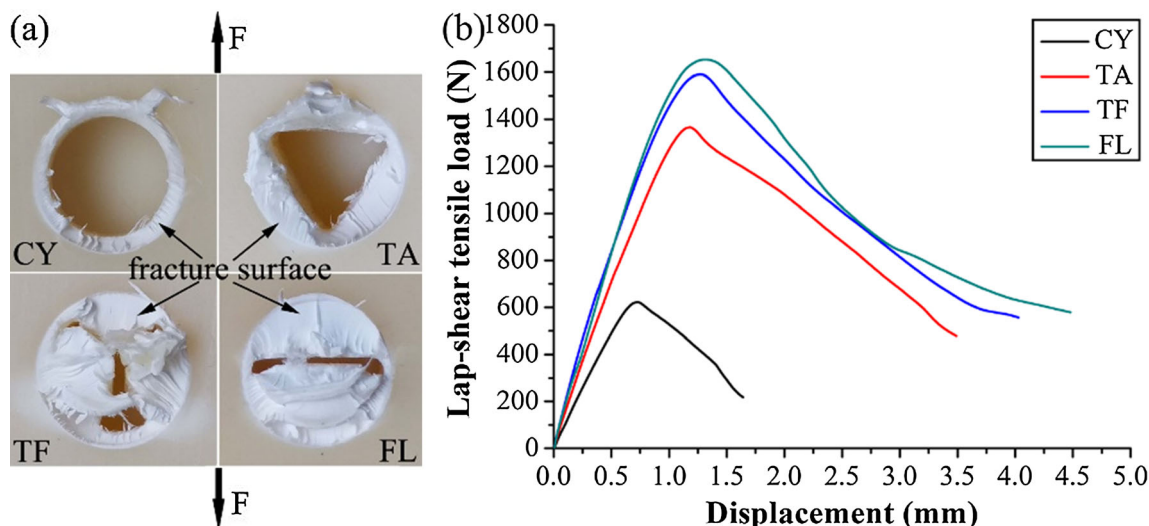


Fig. 15 a The fracture surface and b the typical load versus displacement curves of joints produced by four different pins

fracture mode in the tensile tests. Figure 16 shows the variation of joint lap-shear tensile load and shear strength towards the welding parameters. Although joints produced at N_p 400 and N_p 800 were both defect-free (Fig. 8) and joint dimension increased from N_p 400 to N_p 800 (Fig. 12a), the corresponding lap-shear tensile load slightly decreased with N_p . It was the reason that increased N_p led to stronger shear effect to nugget material, which caused the scission of molecular chains [24]. So joint shear strength which was closely related to the

material microstructure decreased, and the corresponding lap-shear tensile load reduced. At N_p of 1250 rpm, grooves were generated, so the joint fracture load and shear strength decreased heavily, as illustrated in Fig. 16 a. With the increase of R_p the joint fracture load decreased but the corresponding shear strength increased, as can be seen in Fig. 16 b. According to Fig. 12 a, it was obvious that increased bonded region diameter was responsible for the enlargement of joint lap-shear tensile load. However, decreased plunge rate meant

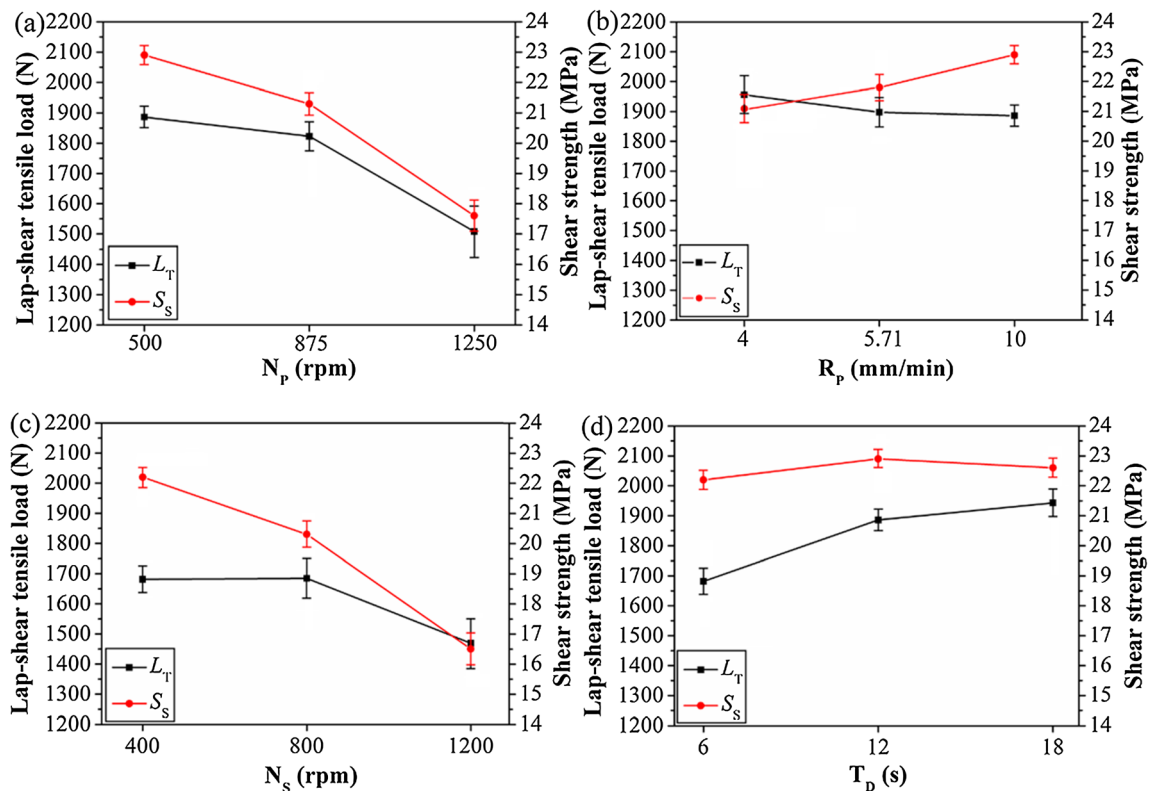


Fig. 16 The lap-shear tensile load and the shear strength of the joints produced under different values: a N_p b R_p c N_s , and d T_D

increased shear effect to the nugget material, which may be the cause to the shear strength decrease. The rotational speed during the stirring phase exerted a significant influence on the joint quality, as can be seen in Fig. 16 c. Joint average shear strength decreased heavily with N_S , which was attributed to the increased groove defect (Fig. 10) as well as serious material degradation resulted from overheat and strong shear effect under higher N_S [24]. Furthermore, it was reported that higher rotational speed led to larger residual stress [25], which may be another cause to the reduction of joint strength. In this case, although the diameter of bonded region increased from N_S400 to N_S1200 (Fig. 12b), the joint lap-shear tensile load varied slightly from N_S400 to N_S800 and then decreased heavily. Figure 16 d shows the variation of joint mechanical performance towards T_D . It was likely that the proper increase of T_D promoted the uniformity of material mixture, so the joint shear strength enlarged from T_D6 to T_D12 . However, further extension of stirring time may result in increased scission of molecular chains, which in turn led to strength reduction. Generally, the shear strength varied slightly with T_D and the corresponding joint fracture load increased towards T_D , which indicated that the appropriate prolongation of stirring time under moderate rotational speed was beneficial to the promotion of joint bearing capacity.

4 Conclusions

ABS sheets were successfully friction stir spot welded by a tool with a flat pin. The influence of welding parameters on joint morphology, dimension, and mechanical performance was investigated. In addition, tools with different pin profiles were adopted and their influences on joint mechanical performance were studied. The main conclusions were listed as follows:

- (1) Spot welds presented bowl-shaped cross-sections due to the decreased frictional heat input along the weld depth. Obvious horizontal and vertical material flow and mixture occurred inside the nugget zone during the welding process.
- (2) Joints with regular initial extrusion ring, flat surface, and sound cross-sectional morphology were produced under moderate N_P and N_S . High N_P and N_S caused secondary extrusion ring, rough surface, and groove defects at the bottom corner of the keyhole. Continuously distributed pores were observed along the boundary of the stir zone when N_S was excessive.
- (3) Increasing the tool rotation number through decreasing the plunge rate or increasing the rotational speed and dwell time had a positive influence on the spot weld diameter.
- (4) The orientation of the keyhole left by the flat pin exerted an obvious influence on the joint lap-shear tensile load. Joints showed larger lap-shear tensile load when the angle between the keyhole orientation and the tensile direction became small.
- (5) Pin geometry exerted a significant effect on the joint dimension and strength. Flat pin produced joints with larger bonded region and fracture load than that fabricated by other pins.
- (6) Joint mechanical performance was significantly influenced by the welding parameters. Excessive rotational speed resulted in heavy decrease of joint lap-shear tensile load and shear strength. Joint fracture load increased while the corresponding shear strength varied slightly with the extension of dwell time under proper rotational speed.

Funding information This study work was supported by the National Natural Science Foundation of China (Grant No. 51475232). This work was supported by Funding for Outstanding Doctoral Dissertation in NUAA (No. BCXJ18-08). This work was supported by the fifth scientific and technological innovation funds in the college of materials science and technology of NUAA in 2017. This was also a project founded by the Priority Academic Program Development of Jiangsu Higher Education Institutions (PAPD).

References

1. Davies G (2003) Future trends in automotive body materials. *Mater Autom Bodies* 8:252–269
2. Sakano R, Murakami K, Yamashita K, Hyoe T, Fujimoto M, Inuzuka M, Nagao Y, Kashiki H (2001) Development of spot FSW robot system for automobile body members. In: *Proceedings of the 3rd International Symposium of Friction Stir Welding*, Kobe, Japan, pp. 645–650
3. Arici A, Mert Ş (2008) Friction stir spot welding of polypropylene. *J Reinf Plast Compos* 27(18):2001–2004
4. Mert Ş, Arici A (2011) Design of optimal joining for friction stir spot welding of poly-propylene sheets. *Sci Technol Weld Join* 16(6):522–527
5. Bilici MK (2012) Application of Taguchi approach to optimize friction stir spot welding parameters of polypropylene. *Mater Des* 35:113–119
6. Bilici MK, Yüklükler AI (2012) Influence of tool geometry and process parameters on macrostructure and static strength in friction stir spot welded polyethylene sheets. *Mater Des* 33:145–152
7. Kurtulmus M (2012) Friction stir spot welding parameters for polypropylene sheets. *Sci Res Essays* 7:947–956
8. Bilici MK, Yüklükler AI, Kastan A (2014) Effect of the tool geometry and welding parameters on the macrostructure, fracture mode and weld strength of friction-stir spot-welded polypropylene sheets. *Mater Tehnol* 48:705–711
9. Bilici MK (2012) Effect of tool geometry on friction stir spot welding of polypropylene sheets. *Express Polym Lett* 6:805–813
10. Bilici MK, Yüklükler AI (2012) Effects of welding parameters on friction stir spot welding of high density polyethylene sheets. *Mater Des* 33:545–550

11. Bilici MK, Yüklükler Aİ, Kurtulmuş M (2011) The optimization of welding parameters for friction stir spot welding of high density polyethylene sheets. *Mater Des* 32:4074–4079
12. Yan Y, Shen Y, Zhang W, Guan W (2017) Effects of friction stir spot welding parameters on morphology and mechanical property of modified cast nylon 6 joints produced by double-pin tool. *Int J Adv Manuf Technol* 92:2511–2523
13. Gonçalves J, Santos JFD, Canto LB, Amancio-Filho ST (2015) Friction spot welding of carbon fiber-reinforced polyamide66 laminate. *Mater Lett* 159:506–509
14. Paoletti A, Lambiasi F, Ilio AD (2015) Optimization of friction stir welding of thermoplastics. *Procedia CIRP* 33:562–567
15. Paoletti A, Lambiasi F, Ilio AD (2016) Analysis of forces and temperatures in friction spot stir welding of thermoplastic polymers. *Int J Adv Manuf Technol* 83(5):1395–1407
16. Lambiasi F, Paoletti A, Ilio AD (2016) Effect of tool geometry on mechanical behavior of friction stir spot welds of polycarbonate sheets. *Int J Adv Manuf Technol* 88:3005–3016
17. Lambiasi F, Paoletti A, Ilio AD (2016) Effect of tool geometry on loads developing in friction stir spot welds of polycarbonate sheets. *Int J Adv Manuf Technol* 87:2293–2303
18. Lambiasi F, Paoletti A, Ilio AD (2016) Friction spot stir welding of polymers: control of plunging force. *Int J Adv Manuf Technol* 90:2827–2837
19. Dashatan SH, Azdast T, Ahmadi R, Bagheri A (2013) Friction stir spot welding of dissimilar polymethyl methacrylate and acrylonitrile butadiene styrene sheets. *Mater Des* 45(6):135–141
20. Yan Y, Shen Y, Zhang W, Hou W (2018) Friction stir spot welding ABS using triflute-pin tool: effect of process parameters on joint morphology, dimension and mechanical property. *J Manuf Process* 32:269–279
21. Yan Y, Shen Y, Hou W, Li J (2018) Friction stir spot welding thin acrylonitrile butadiene styrene sheets using pinless tool. *Int J Adv Manuf Technol* 97:2749–2755
22. Oliveira PHF, Amancio-Filho ST, Santos JFD, Hage E (2010) Preliminary study on the feasibility of friction spot welding in PMMA. *Mater Lett* 64(19):2098–2101
23. Gerlich A, Su P, North TH, Bendzsak GJ (2005) Friction stir spot welding of aluminum and magnesium alloys. *Mater Forum* 29:290–294
24. Capone C, Landro LD, Inzoli F, Penco M, Sartore L (2007) Thermal and mechanical degradation during polymer extrusion processing. *Polym Eng Sci* 47(11):1813–1819
25. Hattingh DG, Blignault C, Van Niekerk TI, James MN (2008) Characterization of the influences of FSW tool geometry on welding forces and weld tensile strength using an instrumented tool. *J Mater Process Technol* 203:46–57

Publisher's note Springer Nature remains neutral with regard to jurisdictional claims in published maps and institutional affiliations.